REACTRF-22-0054

WP4: Integration of Power-to-X into Bornholm's energy system

Feasibility study for Power-to-X production on Bornholm

Version 20230830

Shi You*, Yi Zheng*, Ilaria Sorrenti*

* The authors are all with Department of Wind and Energy Systems, Technical University of Denmark. For further information, please reach shyo@dtu.dk.

THE EUROPEAN UNION
The European Regional Development Fund
Funded as part of the Union's response to the COVID-19 pandemic
Investing in your future

PORT OF ROENNE
Together we create

Danish Board of Business Development

Version Control

Version	Date	Revised by	Description
20230601_0	01.06.2023	Shi You	Structure was created.
20230630_0	30.06.2023	Ilaria Sorrenti	Electrolyser modelling and operation were added.
20230809_0	90.08.2023	Yi Zheng	Analysis on multi-electrolyser operation, heat recovery, and power to ammonia were added.
20230830_0	31.08.2023	Shi You	Finalization

Table of Contents

List of Figures

List of Tables

1. Introduction

Production of green Power-to-X fuels is a completely new type of industry that has not previously existed in Bornholm. In WP4, the objective is to investigate how such a Power-to-X(PtX) plant can be incorporated into Bornholm's energy system from an operational perspective, including the power grid and the district heating system.

2. General description

The investigated PtX facility in Bornholm combines cutting-edge offshore wind farm with water electrolysis technologies to produce green ammonia. Such a facility fulfills multiple purposes, i.e., wind power integration, green hydrogen production, delivery of green ammonia, and a possibility of utilizing the waste heat for local district heating.

2.1 System description

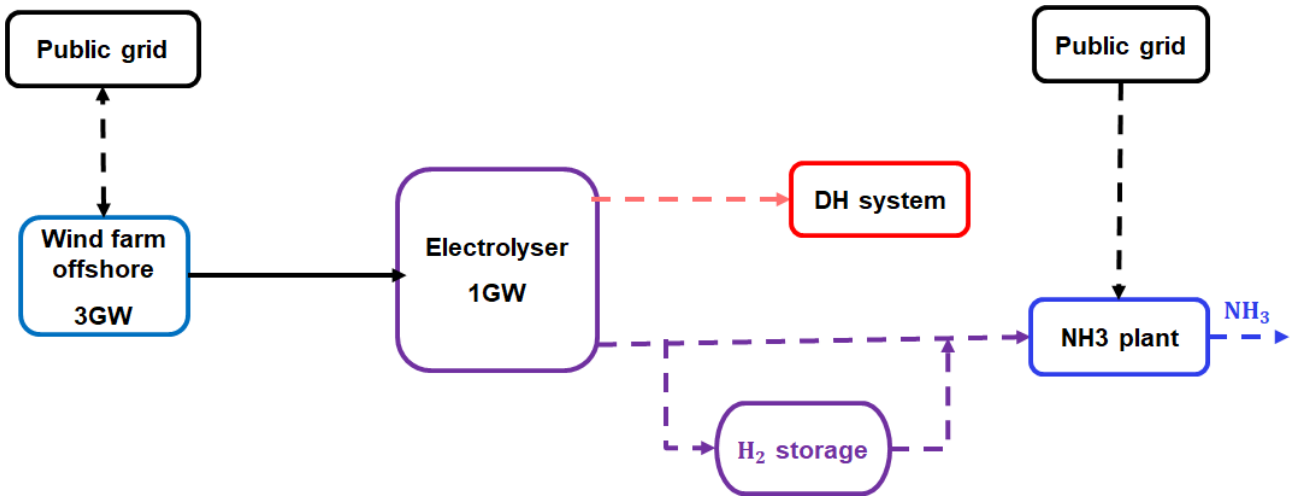

Figure 1 Integration of Power-to-X into district heating and ammonia production systems

Configuration of the PtX facility that is to be investigated is presented in Figure 1, derived from an initial analysis from the investment perspective. The main components within the system are comprised of the following:

a. Offshore wind farm

The 3 GW offshore wind farm on Bornholm consists of many wind turbines installed in strategic locations in the Baltic Sea. These turbines are designed to withstand harsh marine conditions and feature innovative rotor blades and drivetrains for optimal energy conversion. The turbines are equipped with pitch control systems to adjust the blade angles for capturing maximum wind energy, and their hub heights and rotor diameters are optimized to maximise energy capture efficiency. The electricity generated by these turbines is transmitted via underwater cables to the electrolyzer facility onshore.

b. Electrolyzers

The heart of the system is the 1 GW electrolyzer facility, responsible for converting the electricity generated by the wind farm into hydrogen which will be further converted to electro-fuels like ammonia. The electrolyzer facility technology can potentially be either proton exchange membrane (PEM) electrolysis, alkaline

electrolysis (AEL), or solid oxide electrolysis cells (SOEC), or a mixture of them. In this analysis, AEC is selected to constitute the 1GW portfolio due to its level of maturity and relatively low cost.

c. Public grid connection

Once the electricity reaches the on-land electrolyzer facility, it is integrated into the local power grid which now has a rather limited transmission capacity that is below 100MW. Theoretically, connecting the wind farm to the public grid implies a need of addition transmission lines. In this analysis, it is assumed that no additional transmission capacity will be added to the existing grid. In other words, the electrolyser will be purely driven by wind power, as this will guarantee the "source of green power" and correspondingly the derived green products, i.e., hydrogen, heat and ammonia. The residual wind power, i.e., the wind power that can not be used for hydrogen production, indicates the additional capacity of the public grid that is needed to take full use of the wind power.

d. Heat Recovery and District Heating:

During the process of electrolysis, significant amount of heat is generated as a by-product. Therefore, there is a potential to capture and utilize the waste heat to improve both the system economy and renewable utilization. In this study, using the waste heat for the district heating (DH) system in Bornholm is investigated.

e. Green Ammonia Production

The hydrogen produced by the electrolyzer can be combined with nitrogen (obtained from air separation units) using the Haber-Bosch process, producing green ammonia (NH3). The Haber-Bosch reactor operates at specific temperature and pressure conditions to facilitate the efficient synthesis of ammonia. The green ammonia produced is stored in dedicated tanks for further distribution and utilization.

It is assumed that in the PtX Bornholm project, all the hydrogen produced will be used exclusively to produce ammonia. Extensive studies have yet to be conducted to investigate whether ammonia will be produced through a green process (islanded PtX) or if there may be a need to connect the electrolyzer to the power grid.

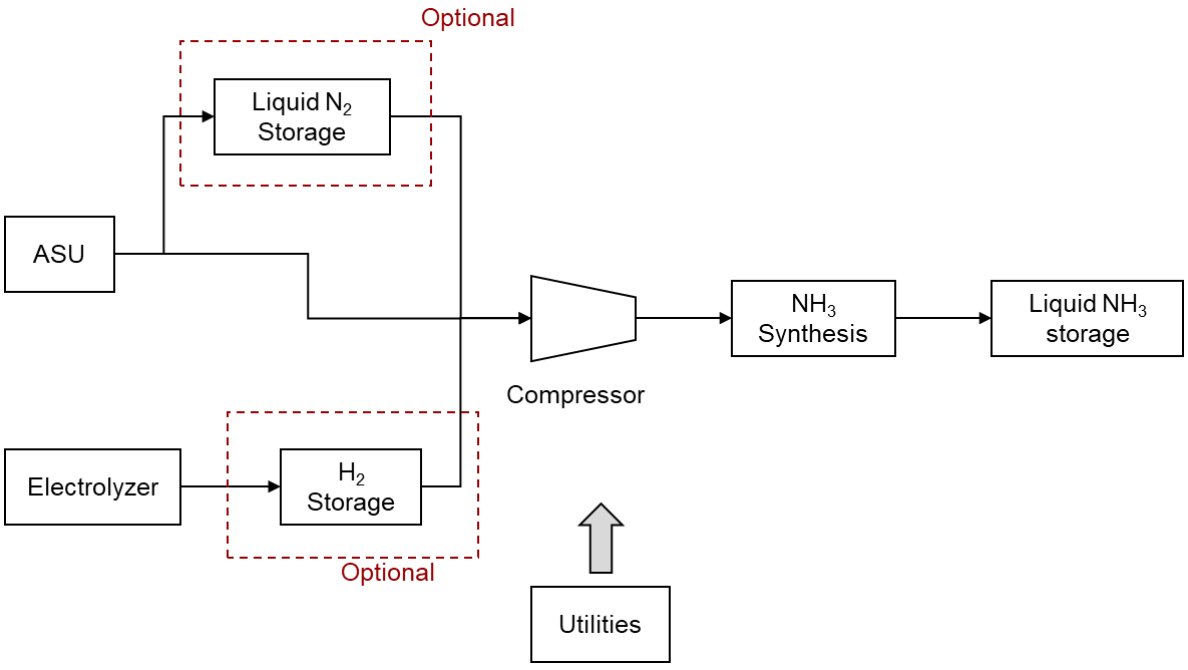

Figure 2 Diagram of ammonia synthesis system

This study models a typical ammonia production system using the Haber-Borch process. The required nitrogen is obtained through an air separation unit that consumes a specific amount of electricity. The obtained nitrogen can be liquefied and stored for the subsequent utilization. The only source of hydrogen is electrolysis, followed by optional hydrogen storage. The two gases are then compressed to a certain pressure for ammonia synthesis. Note that utilities are required to support the operation of most of the components, as indicated in Figure 2.

2.2 Data description

The analysis is based on two major data sources that are provided by the project partners, i.e., wind power data and DH data.

Wind power data from the offshore wind farm on Bornholm is derived based on the hourly wind data used in WP2 (SP379-HH100 Bornholm RPU_OFF_SP379-HH100), considering a 3GW of offshore wind farm in Baltic sea. The received hourly data profile is further converted to a profile with 10 minutes resolution via interpolation to emulate the short-term dynamics, providing valuable insights into the performance and characteristics of the wind resource. Below is a short summary of the data.

Year: The wind power data corresponds to 2021, providing a comprehensive overview of the wind conditions and electricity generation for that specific period. The data available are provided from WP2 for different wind turbines from 2015 to 2021. The simulation is carried out during the year 2016, but it can be easily performed with the other data in Bornholm's folder. Fig. 3 shows the wind profile.

Data Resolution: The wind power data has been calibrated with a resolution of one hour. This means that wind measurements were taken every 10 minutes, allowing for a detailed analysis of the wind patterns and fluctuations throughout the year. An interpolation technique was applied to achieve a higher time resolution of 1 minute for the wind power data from the offshore wind farm on Bornholm. Specifically, a MATLAB tool was utilized to perform the interpolation and generate the data at the desired time resolution. MATLAB provides various interpolation methods suitable for this case, with one commonly used function being the 'interp1' function. The 'interp1' function allows for interpolating data points based on different methods, such as linear interpolation, cubic interpolation, or spline interpolation. Fig. 4 shows a higher resolution wind profile data in order to show the interpolating data.

For the wind power data, the 'interp1' function in MATLAB was applied to the original 1-hour resolution data, utilising an appropriate interpolation method to estimate the values at 10-minute intervals. This interpolation process ensures that the wind power data reflects the fluctuations and characteristics of the wind resource at a higher time resolution, while maintaining the same level of hourly energy production. By employing the interpolation tool in MATLAB, the wind power data from the offshore wind farm on Bornholm was effectively processed and converted to a 10-minute time resolution, allowing for a more detailed analysis of the wind patterns and fluctuations. This interpolated data enables a more accurate assessment of the wind farm's performance, grid integration capabilities, and other related analyses requiring a higher resolution. From the 1-year wind data, two important indicators are identified:

- **Capacity Factor:** The capacity factor, a crucial performance metric for wind farms, is measured as 41% throughout the year.
- **Largest Ramping:** The largest ramping events, which indicate significant changes in wind power generation, are observed in both upward and downward directions.

For 1-year simulation, the largest upward ramping event reached 1.5GW, indicating a sudden increase in wind power generation. In contrast, the largest downward ramping event reached -0.32 GW, presenting a sudden

decrease in wind power generation. These ramping events highlight the variability and dynamic nature of wind resources and their impacts on power generation.

By analysing the wind power data, these metrics provide valuable insights into the performance, variability, and capacity utilisation of the offshore wind farm on Bornholm. This information can be used to optimize operations, assess grid integration capabilities, and evaluate the overall economic viability of the wind farm.

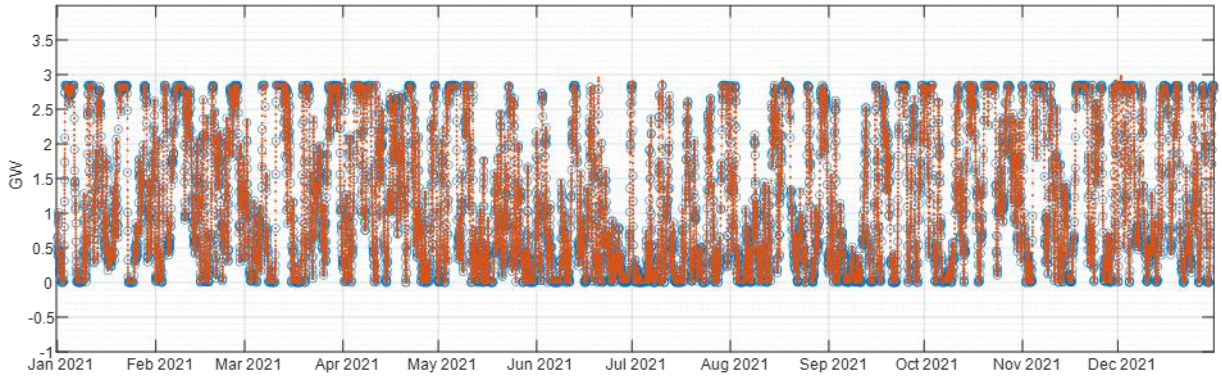

Figure 3 Data of Wind: Lumped data for a 3GW offshore wind farm (source WP2), data resolution

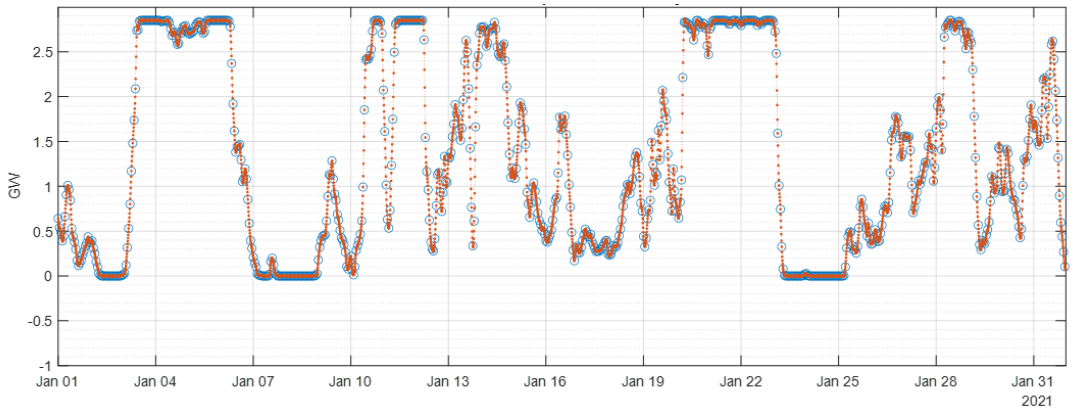

Figure 4 Offshore wind power data for January

Data about DH is provided by the project partner BEOF. As shown in Figure 5, the DH plant is located in Nexø and delivers heat to Svaneke, Nexø, Årsdale, Snogebæk through a regular DH network. In the DH plant, there is a boiler and a heat accumulation tank which are used to meet the heat demand and enhance the system flexibility. The data received is the measured operation data of the DH plant, incl. temperature, pressure, flow, energy, and capacity for one DH network, which can be used to calculate the energy balance and understand how the current DH demand is met the existing DH plant.

.

Figure 5 Locations in Bornholm where data are obtained

Figure 6 shows the supply temperature of the district heating system between Dec. 2021 and Feb. 2022, where the table inside points out the highest supply temperature for the four locations. In general, the supply temperature of the DH system has to be above 70°C in order to meet the end users' demand. During the peak load periods, the supply temperature can get close to 90°C. In terms of the demand of heat, Figure 7 presents the total heat consumed by the studied DH heating system over one year.

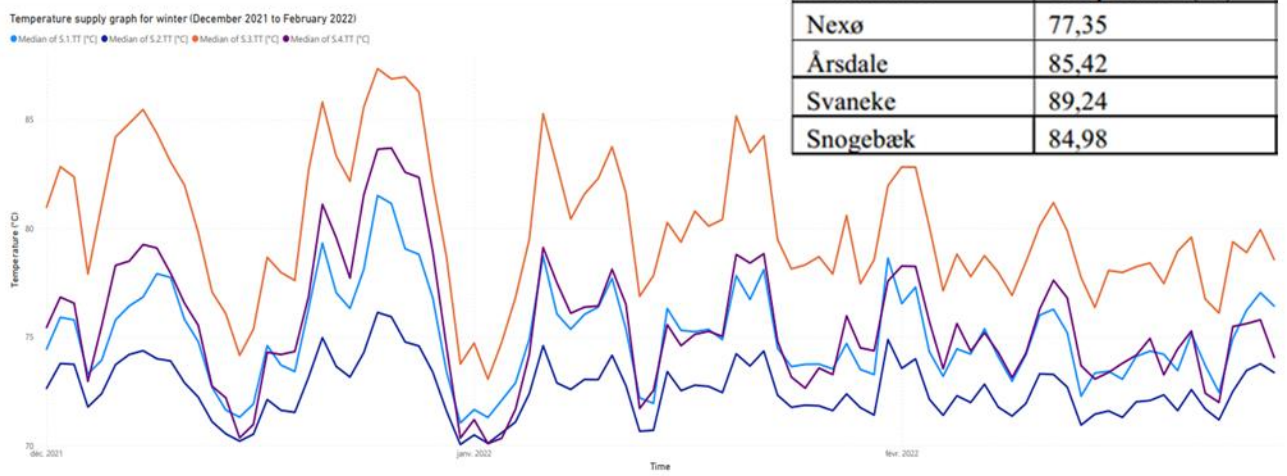

Localisation	Temperature (°C)
Nexø	77,35
Årsdale	85,42
Svaneke	89,24
Snogebæk	84,98

Figure 6 Temperature supply graph for winter (December 2021 to February 2022)

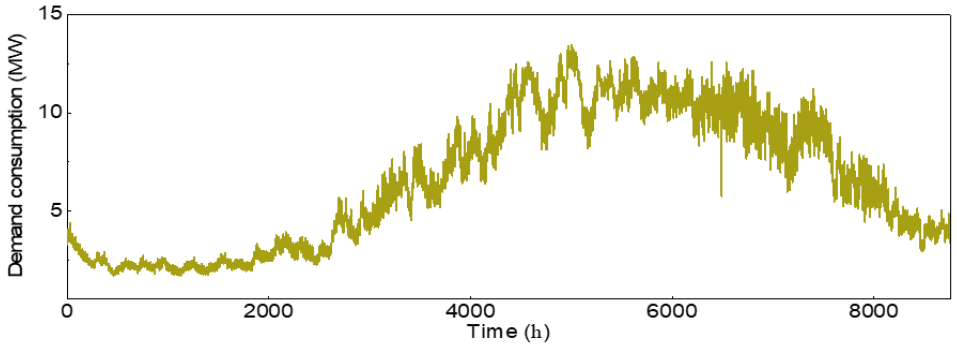

Figure 7 Yearly heat demand with hourly resolution (from May 2021 to June 2022)

3. Model and operation of a multi-unit 1GW electrolyzer plant

3.1 Single unit electrolyzer model

This study uses a classical electrolyzer model that resembles the operation principle of low temperature electrolysers like AEL and PEM electrolyzers. The model is proposed by Ulleberg. The suggested non-linear formulation links voltage and current. The formula shows details it is impossible to find in previous formulations: the voltage and current values and their correlation, having the cons of not being suitable for a system that requires simple linear constraints. As a contribution to the state-of-the-art, the present Ulleberg formulation was piecewise linearized, making it suitable for a Mixed Integer Linear Programming (MILP) formulation.

$$v_{AEL} = v_{rev} + \frac{r_1 + r_2 \cdot T_{AEL}}{A_{AEL}} \cdot I_{AEL} + h_1 \cdot \log\left(\frac{t_1 + \frac{t_2}{T_{AEL}} + \frac{t_3}{T_{AEL}^2}}{A_{AEL}} \cdot I_{AEL} + 1\right) \quad (1)$$

The electrolyzer voltage depends on the input current $I_{AEL}[A]$, cell area $A_{AEL}[m^2]$ and, electrolyzer temperature T_{AEL} [°C] and the reversible voltage $v_{rev}[V]$. The remaining parameters are constants, validated experimentally and shown in [99]. Where, v_{rev} is the reversible voltage in open circuit current mode at standard conditions, i.e., 273 K and 1 atm, equal to 1.229 [V]; Eq. (2) shows the empirical formula for the reversible voltage varying the electrolyzer temperature. Only the electrolyzer steady-state is considered since the operation time lapse is one hour, and the transient lasts for some minutes. It is also assumed that the temperature is constant under operating conditions.

$$v_{rev} = 1.52 - 1.54 \times 10^{-3} \cdot T_{AEL} + 9.52 \times 10^{-5} \cdot T_{AEL}.\ln(T_{AEL}) + 9.84 \times 10^{-8} \cdot T_{AEL}^2 \quad (2)$$

Ulleberg's correlation between voltage and current (V-I) is non-linear and difficult to use as a constraint in an optimization problem. An optimal situation would be a linear relationship between voltage and current (V-I) and power and current (P-I). A piecewise linearization is developed from Ulleberg's formulation to contribute to state-of-the-art advancement. The model developed is for an alkaline electrolyzer (AEL), the most mature technology releasing hydrogen from DC electricity and water, exploiting the redox reaction in a series of cells composed of an anode and a cathode. The AEL operating conditions are 80°C and 15 bar. However, the type of V-I correlation does not favour the choice of a linearization in the current density is domain from 0 to 3500 A/cm^2, as the error would be high. Therefore, the existing domain was split into three sub-domains to reduce the error and find a good compromise between the computational burden of a non-linear and a linear function for the whole current domain. The linearization used linear regression of the available data. The V-I linearization and R-squared are shown in Eq. (3) and Fig. 4. The same procedure is implemented for linearizing the input power varying the current. The same domain partitions were used for the voltage in the electrolyzer shown in Eq. (4) and Fig. 5.

$$v_{AEL}(i_{AEL}) = \begin{cases} 1.18 + i_{AEL} \cdot 5.8 \times 10^{-3}; & \forall i_{AEL} \in [0, 58] \\ 1.53 + i_{AEL} \cdot 4 \times 10^{-4}; & \forall i_{AEL} \in [58, 467] \\ 1.7 + i_{AEL} \cdot 5 \times 10^{-5}; & \forall i_{AEL} \in [467, 3500] \end{cases} \quad (3)$$

$$P_{AEL}(i_{AEL}) = \begin{cases} n_{AEL} \cdot A_{AEL} \cdot 1.5 \cdot i_{AEL} \times 10^{-6}; & \forall i_{AEL} \in [0, 58] \\ n_{AEL} \cdot A_{AEL} \cdot (1.74 \cdot i_{AEL} - 20.42) \times 10^{-6}; & \forall i_{AEL} \in [58, 467] \\ n_{AEL} \cdot A_{AEL} \cdot (1.91 \cdot i_{AEL} - 164.2) \times 10^{-6}; & \forall i_{AEL} \in [467, 3500] \end{cases} \quad (4)$$

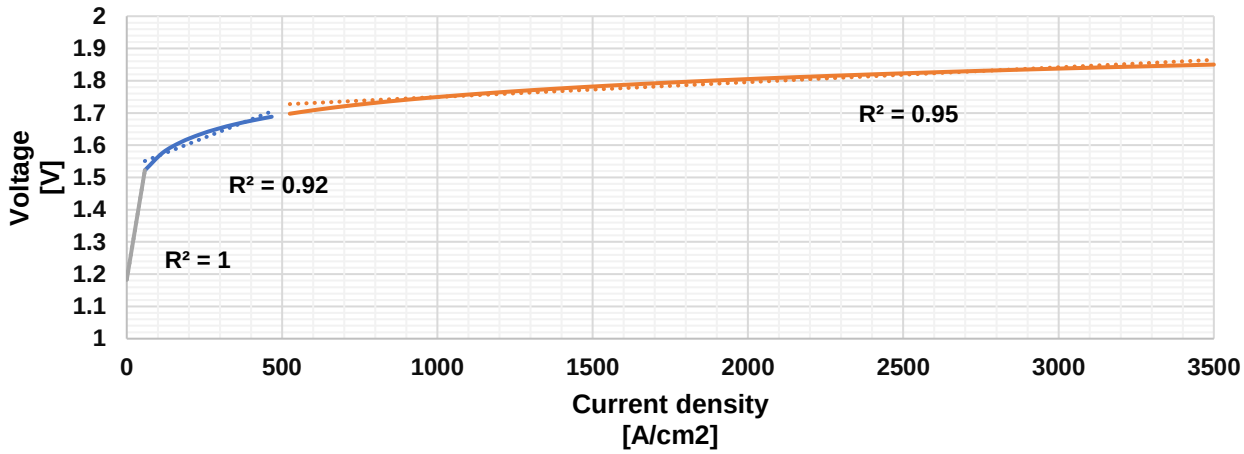

Figure 8 Piece-wise linear approximation of the voltage-current curve

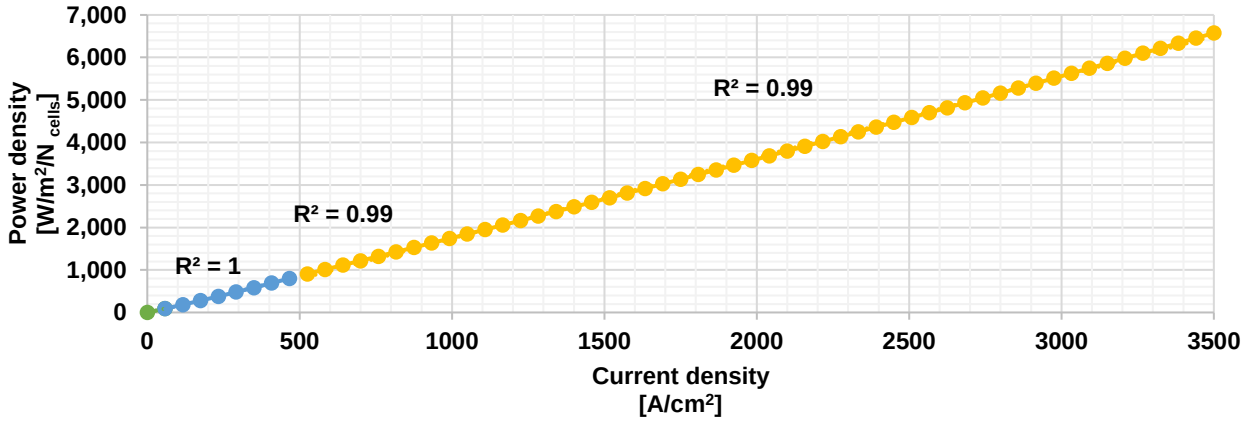

Figure 9 Piece-wise relationship between electrolyzer power density and current density

The non-linear relationship between current and voltage was piecewise linearized, validating the model performance with an R-squared higher than 92%. The piecewise linearization splits the current domain $I_c[A]$ into three sub-domains to make the linearisation error smaller and reduce the computational burden in the optimization. The electrolyzer thermal efficiency η_{el} expresses how far the voltage V is from the thermoneutral voltage V_{tn} shown in Eq. (5). V_{tn} is the voltage drop that drives the cell reaction and provides the heat necessary to maintain a constant temperature.

$$\eta_{AEL} = \frac{v_{tn}}{v_{AEL}} \tag{5}$$

$$\dot{n}_{H_2} = \frac{n_{AEL} \cdot I_{AEL}}{k_{H_2} \cdot F} \tag{6}$$

$$\dot{n}_{H_2} = \dot{n}_{H_2O} = 2 \cdot \dot{n}_{O_2} \tag{7}$$

$$V_{AEL} = \dot{n}_{H_2} \cdot v_{mol_{SC}} \cdot s_{hour} \tag{8}$$

Finally, the hydrogen and water mass flow rate generated by AEL follow Faraday's [100] law in Eq. (6), revealing the current and hydrogen production connection, where k_{H_2} is the amount of substance and F is Faraday constant. Eq. (7) shows the mole oxygen and water flow rate according to the redox reaction. Faraday efficiency is not taken into account in this research.

Eq. (8) shows the hydrogen volume generated in one hour; $v_{mol_{SC}}$ is the volume of a mole in standard conditions $\left(22.4 \times 10^{-3}\left[\frac{m^3}{mol}\right]\right)$ and s_{hour} is the amount of seconds in one hour. The electrolyzer power consumption is the product of current and voltage as $P_{AEL} = V_{AEL} \cdot I_{AEL}$; further piecewise linearized having R-squared higher than 99% validated with appropriate further simulations. The piecewise linearization thus makes it possible to model the AEL component with $P_{AEL} = P_{AEL}(I_{AEL})$, with a linear and straightforward equation not to overload the computational burden in the optimization.

3.2 Operation strategy for the multi-unit 1GW electrolyzer plant

The electrolyzer, with a total power capacity of 1 GW (P_e^{max}), is composed of multiple individual electrolyser modules that operate according to certain strategy. In this analysis, the operation strategy that is selected is so-called “fixed sequence”. This when there is a certain wind power available for any time instance, it will be consumed by the modules one after one, following a pre-defined sequence, until the available wind power is fully converted, or all electrolysers are in full-load operation.

For each individual electrolyser module, a number of operation parameters are further included in the study.

- **Capacity**: a key technological parameter, refers to the nominal electrical power capacity rating of the WE system and is measured in megawatts (MW). The selected capacity of each module would determine how many modules should be there to constitute a 1GW electrolyser plant. For example, if the capacity of a module is 5MW, then the 1GW plant should have 200 modules.
- **Operation range:** the loading level that an electrolyser module can take during normal operation, such as 20-100%.
- **Efficiency**: which indicates the amount of electricity consumed to produce 1 Nm^3 of hydrogen (or equivalent amount of heat measured on a lower heating value basis) when the WE system operates at certain load level power. In this study, the efficiency applied varies when the level of loading varies.
- **Ramp rate:** which indicates the rate at which the electrolyser's loading level can change within a given time period, e.g., 1% per minute.
- **Standby time***:* The duration when the electrolyser is running in an idle operation, i.e., by keeping all the auxiliary units on but having no hydrogen output.
- **Cold Start-up time:** The time it takes to start an electrolyser system from being cold status (i.e., the machine has been shut down and become completely cold) to normal operation.
- **Warm start-up time:** The time it takes to start an electrolyser system from standby to normal operation.

By including the above-mentioned operation parameters into the electrolyser operation model, such as expressed by Eq. (8) that models the ramping capacity of each electrolyser module, the electrolyzer's dynamic performance can be estimated and allows for further investigation of various control strategies.

$$P_{e,t} = \begin{cases} \min\left[\left(P_{e,t_0} + RP_e^{max}\right), P_{w,t}, P_e^{max}\right] & if \;\; P_{w,t} \geq P_{e,t_0} \\ \max\left[\left(P_{e,t_0} - RP_e^{max}\right), P_{w,t}, P_e^{min}\right] & if \;\; P_{w,t} \leq P_{e,t_0} \end{cases} \quad (9)$$

3.3 Heat recovery

The temperature behaviour of an AEL stack is influenced by the equilibrium of thermal energy within it. The changes in temperature over time for the AEL can be represented using a first-order thermal formulation.

$$C_{AEL}\frac{dT_{AEL}}{dt} = \dot{Q}_{pro} - \dot{Q}_{loss} - \dot{Q}_{cool} = N_{cell}\mathrm{I}_{\mathrm{AEL}}V_{AEL}(1-\eta_{\mathrm{AEL}}) - \frac{T_{AEL}-T_a}{R_{heat}} - \dot{Q}_{cool} \quad (10)$$

Here, C_{AEL} denotes the combined thermal capacitance of the Alkaline Electrolyzer (AEL), while N_{cell} represents the quantity of cells contained within the AEL. The system efficiency is denoted by η_{AEL}, T_a signifies the ambient temperature, and R_{heat} heat represents the heat resistance specific to the AEL. The cooling power, $\dot{Q}_{cool}$ can be defined as follows:

$$\dot{Q}_{cool} = \dot{m}_{cool}c_{H2O}(T_{AEL}-T_{cin})\left(1-e^{-\frac{UA}{\dot{m}_{cool}c_{H2O}}}\right) = f(T_{AEL},\dot{m}_{cool}) \quad (11)$$

Here, $\dot{m}_{cool}$ corresponds to the mass flow rate of the cooling water, while c_{H2O} signifies the specific heat capacity of the cooling water. T_{cin} represents the inlet temperature of the cooling water, and UA stands for the heat transfer coefficient of the heat exchanger.

Equation (11) elucidates that $\dot{Q}_{cool}$ is contingent on both the temperature of the AEL and the mass flow rate of the cooling water. This relationship holds under a defined configuration of the cooling system, where UA and T_{cin} are known. By regarding $\dot{m}_{cool}$ as an adjustable parameter, the cooling power becomes modifiable, allowing for the deliberate regulation of the AEL's temperature to a targeted value. To achieve this objective, the present study introduces a temperature-stabilizing controller designed to manage the temperature and maintain it at the desired set point.

To uphold the desired target value, a closed-loop controller is formulated utilizing the proportional-integral (PI) regulation approach. The fundamental concept involves feeding the discrepancy between the current temperature and its intended reference into the PI regulator. This process yields a scaling factor denoted as λ, which spans from 0 to 1, influencing the mass flow rate. The mathematical representation of this controller is captured in equation (12). Subsequently, considering an initial delay associated with regulating the valve's effect on altering the mass flow rate, the cooling water's mass flow can be ultimately defined using equation (13). At a state of equilibrium, the PI regulator guides the actual temperature to faithfully track its reference, thereby proficiently upholding the temperature at the predetermined set point.

$$\lambda = (T_{AEL}-T_{REF})(k_p + \frac{k_i}{s}) \quad (12)$$

where T_{REF} is the temperature set point; k_p and k_i are the control parameters of the PI regulator.

$$\dot{m}_{cool} = \rho_{cw}k_n\lambda\frac{1}{1+t_d s} \quad (13)$$

Here, ρ_{cw} represents the density of water; k_n signifies the peak volume flow rate of the cooling water; and t_d stands for the time constant linked to the valve adjustment procedure.

3.4 Power to Ammonia

The ammonia synthesis system mainly consists of four components: utilities, air separation unit, a compressor, and an ammonia synthesis plant (ASP). Each of the components bears distinct dynamic properties, for example as shown in Table 1.

	Working prerequisites	Start-up time	Working range	Ramping rates	Power consumption
Utilities	None	3h	100%	None	1% Nominal power
ASU	Utility on	36-48h	75%-100%	None	2% Nominal power
Compressor	Utility on	1h	75%-100%	1%/min	5% Nominal power
NH_3 synthesis plant	Utility, ASU, Compressor on (Hot standby: utility on)	Cold start: 12h Hot start: 0-4h (depending on standby time)	20%-100%	3%/min	None

Table 1 Operational parameters of the components within the ammonia synthesis system

Only if the utilities are on do the remaining devices operate normally. The utilities consume 1% of the nominal power (1GW in this case) to support the operation of other device. They can be shut down to save electrical energy. The restart, however, takes nearly three hours. The air separation unit has an even longer start up time and consumes power of 2% nominal power. The compressor has a faster start up speed, which is limited by the upward/downward ramping rates. It consumes even more electrical power. Finally, the NH_3 synthesis plant only works when all other devices are operating. It has a working range of 20% to 100%, implying that the ammonia production rate can be adjusted to accommodate the input hydrogen. Nevertheless, the production rate change is limited by the ramping rates, like the case of the compressor. It should be noted that the NH_3 synthesis plant can be put on standby as long as the utilities are working. Transition from standby to production (Hot start) takes less time than cold start (from off state to display).

The operation of an ammonia synthesis system refers to the efficient management of all the involved components that can ensure normal operation and optimize the overall ammonia production.

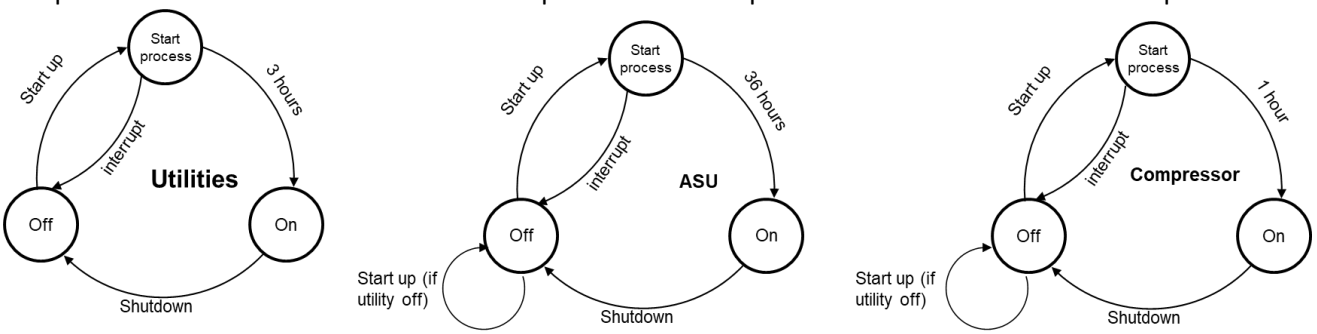

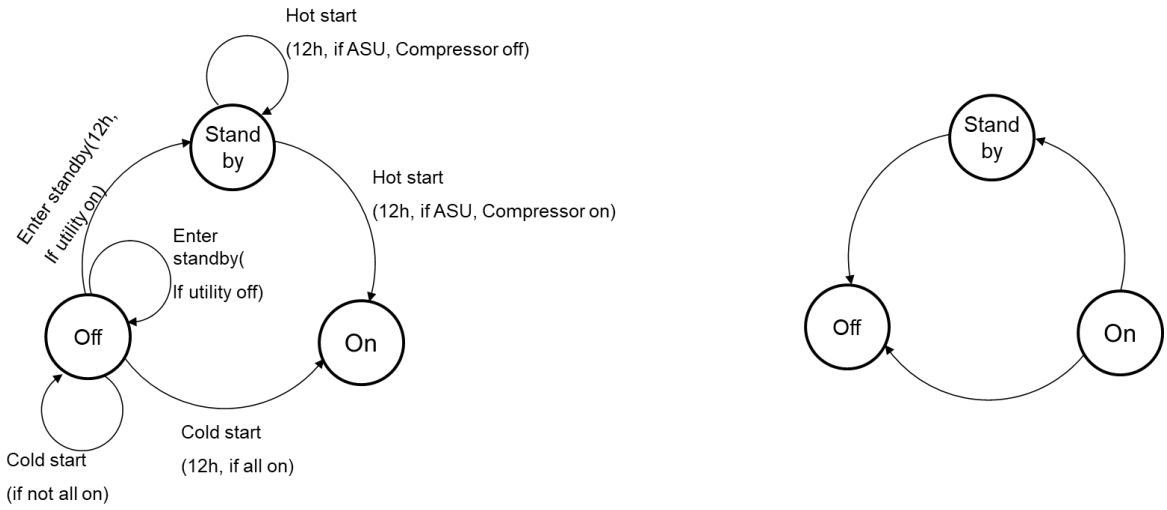

Figure 10 State machine diagram for the components within the ammonia synthesis system

The state machine diagrams of the mentioned components are shown in Figure 10, which highlights the state transitions of each component. For example, a start up demand makes the utilities shift from off state to start process, and if the component has been in starting process for 3 hours, its state becomes on. Similar logic applies to air separation unit and compressor with different parameters. Note that the start up command may not work if the working prerequisites are not satisfied. For instance, if utilities are in off state, the compressor can not be started. The state machine diagram of the ASP presents a more complex structure due to the introduction of a standby state and more working prerequisites. The entering standby command puts the synthesis plant in standby state from off state given certain conditions. To summarize, the state machine diagrams offer a direct description of the ways to manage these components and present the related prerequisites. These operational rules enable researchers to consider more operational details and restrictions from the ammonia synthesis system.

3.5 Operational strategy for the hydrogen to ammonia process

The operational strategy aims to increase the production of ammonia, given specific hydrogen input. This study particularly focuses on the cases without hydrogen storage, which results in a more dynamic hydrogen input and more necessity of flexible operation of ammonia synthesis. In the case of stable hydrogen input, the ASP will also work in a stable way.

Three strategies are proposed as follows:

- Strategy 1: Utility, ASU, and compressor always on; ignore the lower limits of ASP.
- Strategy 2: Utility, ASU always on, shutdown compressor and put ASP into standby if hydrogen is insufficient. Restart the compressor and ASP when the hydrogen supply reaches an acceptable level.
- Strategy 3: ASU is always on. Based on strategy 1, if ASP has been on standby for a certain time, shut down the utility and ammonia plant.

Strategy 1 ensures that the supporting units, including Utilities, ASU, and compressor, are always working, regardless of the hydrogen input. They will be on even if ammonia synthesis is not in operation. Apart from this, we ignore the lower working limit of ammonia synthesis, 20% of its nominal capacity. The ammonia production is only limited by the ramping limits. These settings will lead to an ideal scenario and result in the most ammonia production.

Strategy 2 offers a more realistic method to operate the system. A key difference is that the ASP is put on standby if the hydrogen input is insufficient, i.e., lower than 20% of its nominal value. The plant will restart if there is enough hydrogen. Considering the start-up time of the involved component, we only shut down the compressor when ASP is on standby, while the utility and ASU are always on. Because the start up time of the compressor is generally longer than the ASP, it is the ASP dominates during the starting process.

Strategy 3 improves strategy 2 by completely shutting down the ASP if it has been on standby for a long time. Although the ASP consumes minor energy on standby, the utilities and ASU are still working and consuming electricity. To reduce energy consumption, the utilities are shut down if the ASP stops working. The ASU still works to avoid a restart that takes a long time. The potential problem with this strategy is that the ASP requires a long time to conduct a cold start, which may lead to hydrogen curtailment.

The performance of these strategies will be further discussed in the next section.

4. Integration analysis

This section presents the simulated results delivered by this investigation, including the definitions of the scenarios, the analysis of hydrogen production, electricity output, heat generation and ammonia production.

4.1 Scenario description

In this study, two scenarios are designed to investigate the operational difference between different configurations of the 1GW electrolyser plant.

	Scenario 1	**Scenario 2**
Total capacity of offshore wind	3 GW	3 GW
Electrolyzer capacity	5 x 200MW	20 x 50MW
The initial temperature of stack	56.4 °C	56.4 °C
Cooling water temp.	10 °C	10 °C
Mass flow rate of cooling water for one module	16E+05 kg/h	4E+05 kg/h
Efficiency	Variable	Variable
Operation range	20-100%	20-100%
Ramping rate (operation mode)	10% per min	10% per min
Start-up time (cold)	60 mins	60 mins
Start-up time (warm)	< 10mins	< 10min
Time resolution	10 mins	10 mins

Table 2 Definitions of the two scenarios

As shown in Table 2, both scenarios include a 3GW offshore wind farm and a 1GW electrolyser system that is powered by the offshore wind. Scenario 1 uses 5 electrolyzer with the capacity of 200 MW while in scenarios 2, 20 electrolyzers of 50 MW are deployed. By defining these two scenarios, we aim at comparing the final system performance and show the difference of using large and small electrolyzer stacks. Except the mass flow rate of cooling water for each module, the two scenarios share same parameters.

4.2 Hydrogen production and power exchange with the electricity grid

This section introduces the results regarding the wind/electrolysis process. The heat integration and ammonia production will be discussed later in section 4.3 and section 4.4 respectively. As shown in Table 3, scenario S1 and S2 generally result in very similar results. The overall yearly hydrogen production in scenario S1 is 102.0 kton, which is only 0.6kton less than that in scenario S2. The difference is caused by a combination of the varying nature of electrolysis efficiency and the utilization rate of wind energy. The efficiency increases as the electrolyzer load level reduces. Thus, it can be inferred that scenario S1 has a higher average electrolysis efficiency because of the larger capacity of electrolyzer module. For the identical power input, the larger modules have lower load level on average. However, the total electricity consumption in scenario S2 is higher, as the small modules are able to consume more electricity. For example, 30 MW wind power can be used by a 50 MW module while it cannot be utilized by a 200 MW module as it is outside the working range (40 MW-200 MW in this case).

More waster heat is produced in scenario S2 where averagely the electrolysis efficiency consumption is lower and the overall electricity is higher. Both factors contribute to more waster heat generation. Also, more heat is recovered in scenario S2.

	S1	S2
Module number and capacity	5 x 200MW	20 x 50MW
H2 production (kton)	102.0	102.6
El consumption (GWh)	5650.7	5669.9
Waste heat produced (GWh)	1581.7	1590.5
Waste heat recovered (GWh)	1483.2	1485.7
Rate of waste heat recovery %	93.8	93.4
Electricity curtailed / exported (GWh)	5237.7	5217.5

Table 3 Key operational results of the two scenarios

It is observed that the curtailed electricity in scenario S1 is more than S2, as a result of lower electricity consumption in S1. However, the difference is minor. Figure 11 and Figure 12 further shows the curtailed power in S1 and S2 respectively. The profiles in these two figures do not show significant difference, implying that the configuration of electrolysis system has little influence of power curtailment in the studied case.

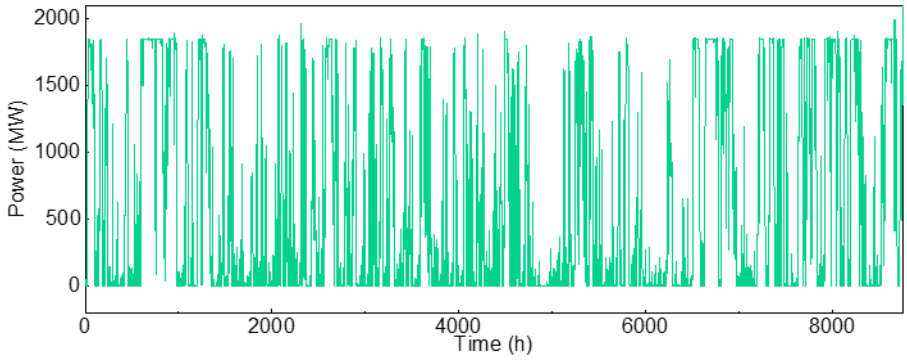

Figure 11 Curtailed electricity in scenario 1

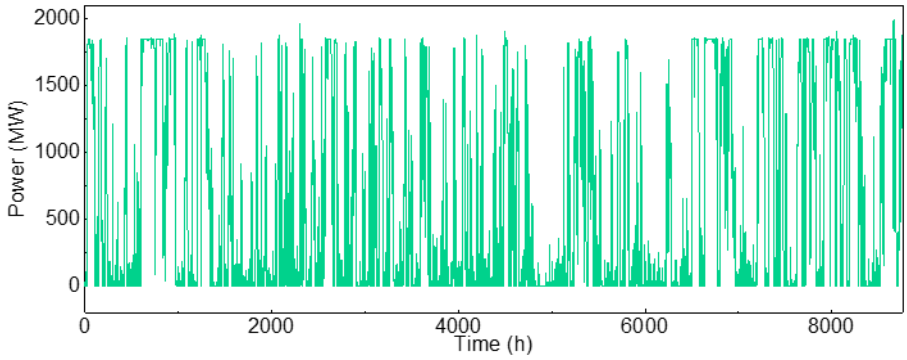

Figure 12 Curtailed electricity in scenario 2

Figure 13 and Figure 14 illustrate the hydrogen production and heat recovery in scenario S1. The maximal hydrogen production rate reaches 200000 Nm^3/h. No significant difference of hydrogen production rate is observed in terms of different seasons. Also, the profile suggests that ramping rates are not key factor limiting the change in hydrogen production rate. The heat recovery shows similar trends as the hydrogen production curve. The maximal heat recovery power reaches around 260 MW, accounting for 26% of the overall capacity of the electrolysis units.

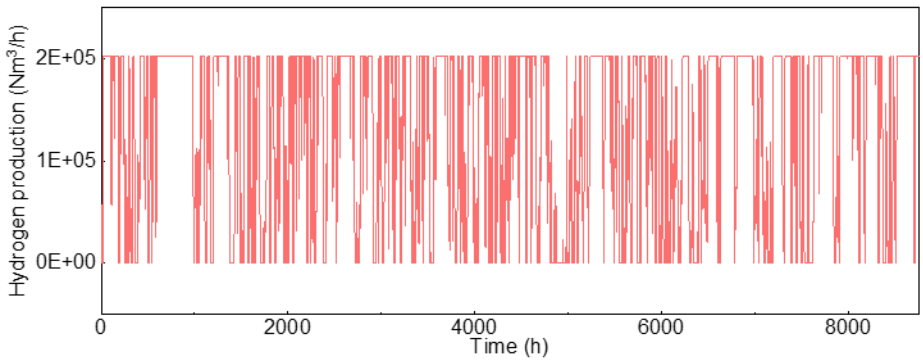

Figure 13 Annual hydrogen production from the electrolyzers in scenario 1

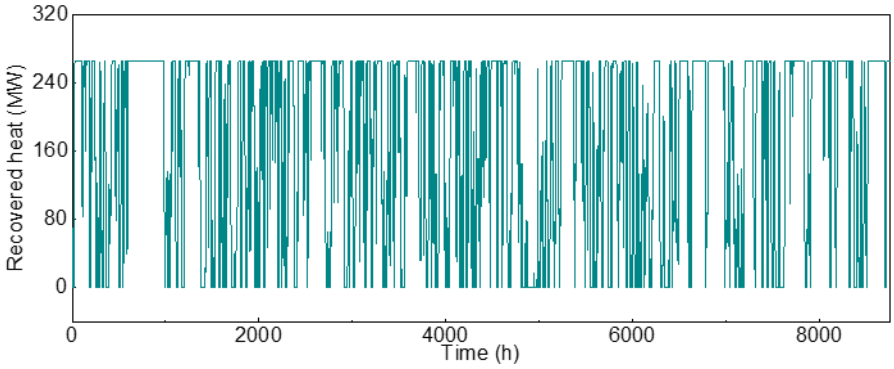

Figure 14 Annual heat recovery from the electrolyzers in scenario 1

In scenario S2, the hydrogen production and recovered heat are very similar to S1, as illustrated in Figure 15 and Figure 16.

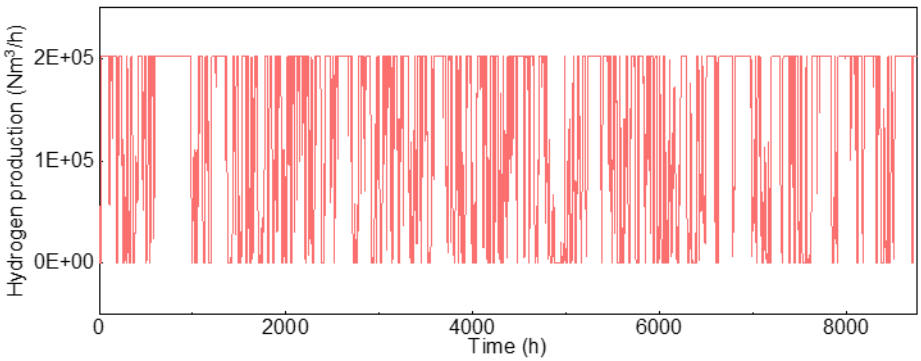

Figure 15 Annual hydrogen production from the electrolyzers in scenario 2

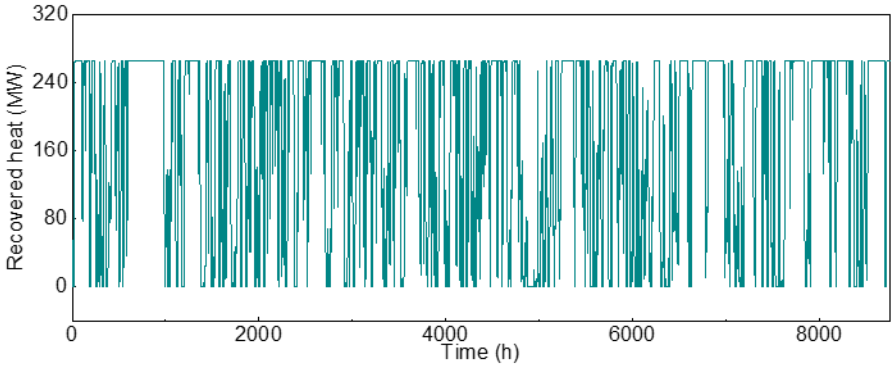

Figure 16 Annual heat recovery from the electrolyzers in scenario 2

The next two figures describe the operational details for each module within the electrolysis system. Figure 17 shows the state transitions of the five modules in scenario S1. The operational state can be -1, 0, 1, which are corresponding to off, standby and production state, respectively. From Figure 17, we can see that module 1 is in production state in most of time, while module 5 undergoes frequent shutdown and standby. This is

because the operational strategy of the five modules prioritizes module 1. The wind energy is firstly utilized by module 1, and the remained energy is distributed to other modules. Module 5 frequently faces insufficient energy input, thereby leading to a smaller load factor.

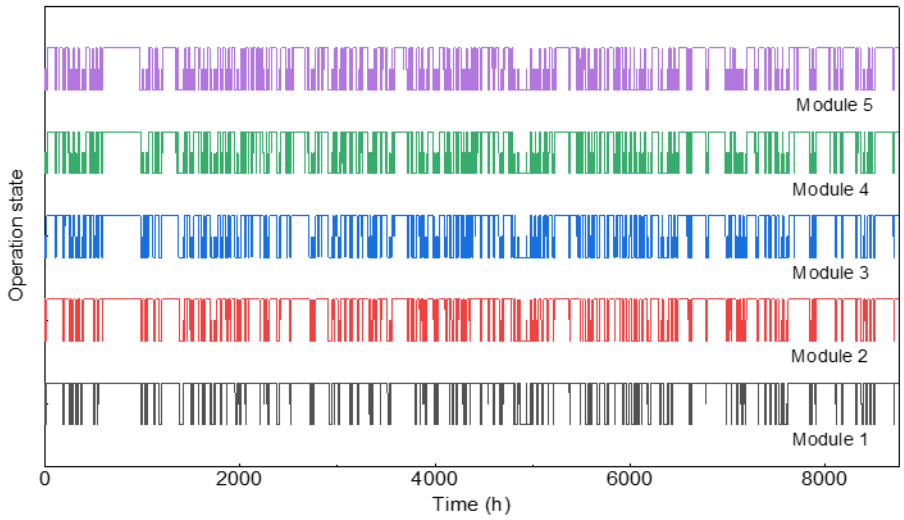

Figure 17 Operational state of each module in scenario 1

The operational details of the five modules are displayed in Table 4. Again, it is found that the stop times (completely shutdown) increases from module 1 to 5, while the load factor decreases. The load factor of module reaches 81%, significantly higher than that of module 5, 51%. The electricity consumption in the table describes the wind power distributed to each module. Obviously, module 1 consumes more electricity than the others. These statistical results highlight the characteristics of the proposed operational strategy for multiple electrolyzers.

	Stop times	Load factor %	El_consumption (GWh)
Module 1	158	81	1419.6
Module 2	186	72	1256.0
Module 3	189	63	1097.1
Module 4	190	56	984.0
Module 5	197	51	894.4

Table 4 Operational indicators of each electrolyzer module in scenario 1

Figure 18 and Table 5 depict the state transition and operational results in scenario 2. Basically, the same conclusion can be obtained: modules that are in the tailor of the electrolyzer sequence undergoes more state transitions and consumes less energy. Module 1 has the highest load factor while module 20 has the lowest.

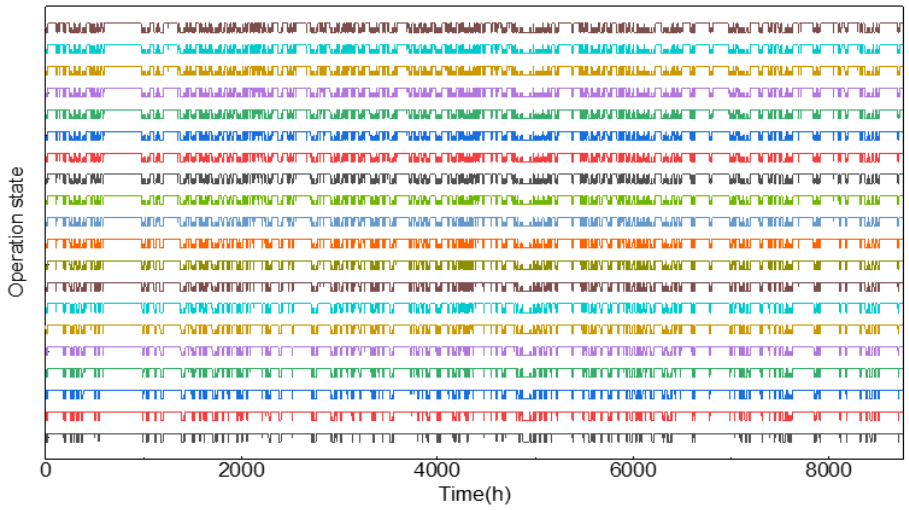

Figure 18 Operational state of each module in scenario 2

Item	Stop times	Load factor %	El_consumption (GWh)
Module 1	146	86	375.1
Moudle 2	164	82	360.5
Module 3	172	82	351.7
…	…	…	…
Module 20	204	49	215.2

Table 5 Operational indicators of each electrolyzer module in scenario 2

The above analysis demonstrates the effectiveness of the electrolyzer in describing the state transitions. Besides, it highlights the characteristics of the proposed strategy: modules share different priorities and has distinct load factor.

4.3 Integration analysis for heat

This section calculates the temperature variation and the key parameter for district heating system, temperature of the outlet cooling water.

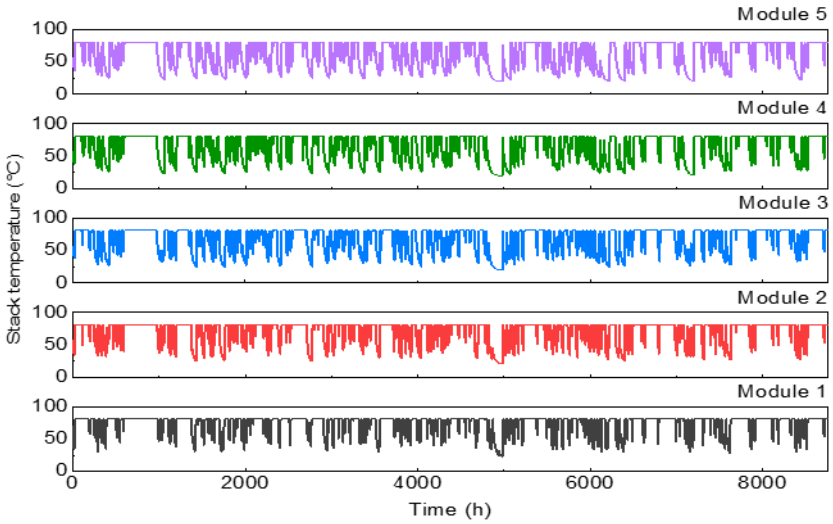

Figure 19 Stack temperature variation of each module in scenario 1

Figure 19 illustrates the temperature variation of the modules in scenario 1. The algorithm (12) is applied to control the temperature. It is observed that all the module temperature is controlled to be under the nominal operational temperature, 80℃. Apart from this, the average operational temperature decreases from module 1 to 5, as a result of decreasing heat generation, which is proportional to the electricity consumption. The cooling system uses a water with inlet temperature of 10℃. We find that the outlet water temperature in this scenario is still below 40℃. Therefore, although the overall heat recovery outweighs the heat demand in Bornholm, the temperature of water has not met the requirement of the district heating system. The water temperature is expected to be above 70℃ as shown by the historical data in Figure 6.

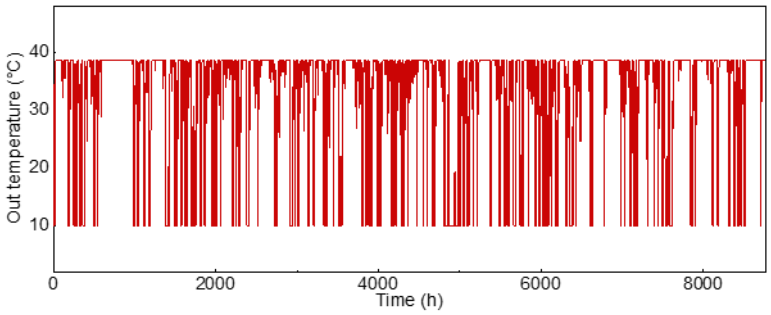

Figure 20 Temperature variation of the outlet cooling water in scenario 1

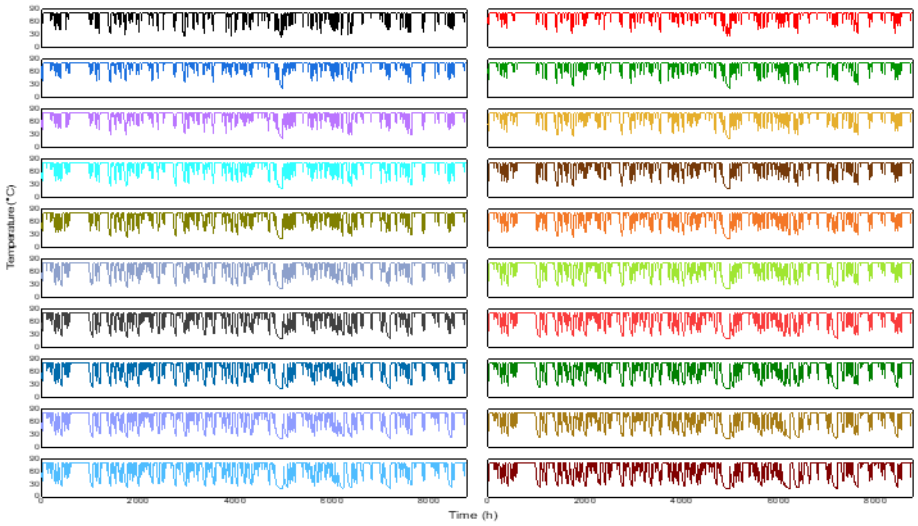

Figure 21 Stack temperature variation of each module in scenario 2

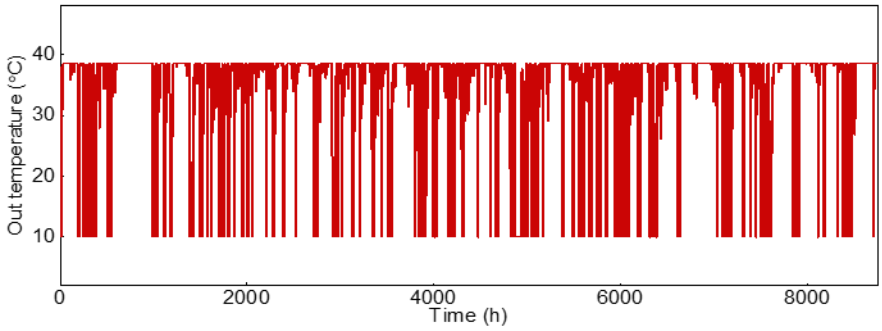

Figure 22 Temperature variation of the outlet cooling water in scenario 2

Figure 21 and Figure 22 present the results for scenario 2. Using more electrolyzer modules does not lead to any significant difference. The supplying temperature to district heating system is still below 40℃.Figure 22

4.4 Potential for ammonia production

Here, we discuss the influence on ammonia production from electrolyzer configuration and the ramping limits of ASP. The difference of using the strategies mentioned in section 3 is also presented. The following tables show the system operational performance.

Strategy	Annual ammonia production (kt)	Utility energy consumption (MWh)	ASU energy consumption (MWh)	Compressor energy consumption (MWh)	Overall electricity consumption (MWh)	Unused hydrogen (kt)
1	579.59	90229	180459	451148	721837	0.03
2	552.42	90229	180459	328612	599302	4.82

3	468.57	68364	180459	328612	577436	19.62

Table 6 Energy consumption, hydrogen curtailment and ammonia production of the ASP considering different strategies (Hydrogen comes from the electrolysis system with **5×200 MW** electrolyzers, and the ramping limit of ASP is **3%/min**)

Table 6 shows that the overall ammonia production is reduced from strategy 1 to 3, as a result of the ideal assumption in strategy 1: the ASP can consume any hydrogen input. Only 0.03 kt hydrogen is not used, and the curtailed hydrogen is caused by the ramping limits. For example, if hydrogen increases by 50% of nominal input within a time step, the ASP cannot consume all the hydrogen due to limited following ability. Note that significant energy is used by the utilities, ASU, and compressor to support the operation of the ASP.

Strategy 2 results in less ammonia production and more unused hydrogen. In this case, hydrogen cannot be consumed if it is below the lower hydrogen input limit of the ASP, thus leading to a large amount of hydrogen curtailment. Also, the ASP is frequently put on standby. It takes a few hours for the hot start of the ASP and during the starting process, hydrogen cannot be used, causing some curtailment. We also observe that strategy 2 reduces the compressor energy consumption because the compressor is shutdown if the ASP is in standby.

Strategy 3 yields a large decrease in ammonia production and a greater surplus of hydrogen. The ASP is occasionally completely shutdown, together with the compressor and utilities. Once the ASP is off, it takes considerable time to restart, and during the long starting process, hydrogen cannot be utilized. Currently, the only benefit of strategy 3 is the possibility of shutting down utilities, which is expected to lower the energy consumption. However, the energy savings are minor, as shown in Table 6, making strategy a less attractive option.

Overall, strategy 1 is limited by the ideal assumption of the ASP operation and strategy 3 leads to an inefficient operation. Strategy 2 is more likely to be reliable and effective for the management of the ASP system.

Furthermore, we discuss the influence of different hydrogen profile, although it has been shown the overall hydrogen production is very similar given the two settings of electrolyzers. Table 7 presents the results for the case with 20×50 MW electrolyzers. One can observe that the overall ammonia production is increased for all three strategies and the curtailed hydrogen is reduced. Although the difference is slight, we conclude that smaller electrolyzer stacks contribute to a more stable hydrogen output profile, thereby reducing the hydrogen curtailed because of dynamic limitations. Note that the energy consumption for the compressor is increased, implying less standby of the ASP, which supports the fact that hydrogen input is more stable.

Strategy	Annual ammonia production (kt)	Utility energy consumption (MWh)	ASU energy consumption (MWh)	Compressor energy consumption (MWh)	Overall electricity consumption (MWh)	Unused hydrogen (kt)
1	581.29	90229	180459	451148	721837	0.02
2	557.73	90229	180459	335213	605902	4.18
3	479.29	69842	180459	335213	585515	18.02

Table 7 Energy consumption, hydrogen curtailment and ammonia production of the ASP considering different strategies (Hydrogen comes from the electrolysis system with **20×50 MW** electrolyzers, and the ramping limit of ASP is **3%/min**)

In the last two cases, we discuss the potential influence of the ramping rate of the ASP. Reducing the ASP ramping rate to 0.3%/min, Table 8 shows the results when 5×200 MW electrolyzers are utilized and Table 9 shows results for 20×50 MW electrolyzers. It is found that the decrease of the ramping rate lead to drops of ammonia production for all three strategies. Besides, the unused hydrogen is increased. For example, ammonia production in Strategy 1 is 566.14 kt given the ramping rate of 0.3%/min, which is 13.45 kt less than the 579.59 kt if the ramping rate is 3%/min. This observation highlights the importance of fast ramping rate of the ASP, especially for the cases without hydrogen storage.

Strategy	Annual ammonia production (kt)	Utility energy consumption (MWh)	ASU energy consumption (MWh)	Compressor energy consumption (MWh)	Overall electricity consumption (MWh)	Unused hydrogen (kt)
1	566.14	90229	180459	451148	721837	2.4
2	529.67	90229	180459	328612	599302	8.84
3	445.86	68364	180459	328612	577436	23.63

Table 8 Energy consumption, hydrogen curtailment and ammonia production of the ASP considering different strategies (Hydrogen comes from the electrolysis system with **5×200 MW** electrolyzers, the ramping limit of ASP is **0.3%/min**)

Finally, we investigate the influence of ramping rate when 20×50 MW electrolyzers are adopted. Again, we find that ammonia production reduces and hydrogen curtailment increases. Compared to the case with ramping rate of 3%/min, the ammonia production is reduced by 12.06 kt in scenario 1. The reduction of ammonia production in this case is less than the one with 20×50 MW electrolyzers, as a result of more stable hydrogen supply in this case.

Strategy	Annual ammonia production (kt)	Utility energy consumption (MWh)	ASU energy consumption (MWh)	Compressor energy consumption (MWh)	Overall electricity consumption (MWh)	Unused hydrogen (kt)
1	569.23	90229	180459	451148	721837	2.15
2	535.98	90229	180459	335213	605902	8.01
3	457.1	69842	180459	335213	585515	21.93

Table 9 Energy consumption, hydrogen curtailment and ammonia production of the ASP considering different strategies (Hydrogen comes from the electrolysis system with **20×50 MW** electrolyzers, the ramping limit of ASP is 0.**3%/min**)

To summarize, we have the following findings:

- Strategy 2 outperforms the other strategies due to its reliability and efficiency.

- If smaller electrolyzer modules are utilized, the hydrogen output would be more stable, leading to higher ammonia production.
- Increase of the ramping rate of the ASP benefits the ammonia production and helps using more hydrogen in a dynamic way.

5. Other investigations carried out

During the process of performing this feasibility analysis, several additional works have been carried out to add some in-depth knowledge to related subjects. These include,

[A] C. Huang, X. Jin, Y. Zong, S. You, C, Træholt, Y. Zheng, "Operational flexibility analysis of alkaline electrolyzers integrated with a temperature-stabilizing control", Presented in the 8th International Conference on Sustainable and Renewable Energy Engineering, Nice, France, May 12, 2023.

The work, as shown in Figure 23, developed a temperature regulation strategy for improving the operational flexibility of AEL by controlling the cooling circuit. The work provided a basis for estimating the temperature variation of AEL during operation, which can be extended to investigate various heat recovery methods.

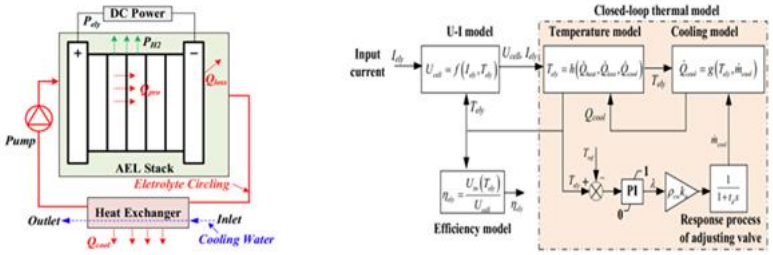

Figure 23 Thermal management for electrolyser stack via cooling regulation

[B] Y. Zheng, C. Huang, J. Tan, S. You, Y. Zong, C. Træholt, "Off-grid Wind/hydrogen Systems with Multi-electrolyzers: Optimized Operational Strategies", submitted to Energy Conversion and Management, 2023 (Under review)

The work investigated three operation strategies for performing control and dispatch of a multi-electrolyser system, so-called fixed sequence, sequence rotation and optimal sequencing. The results, as given in Figure 24, demonstrate the value of applying optimization to this problem, which results in the least cost of hydrogen production.

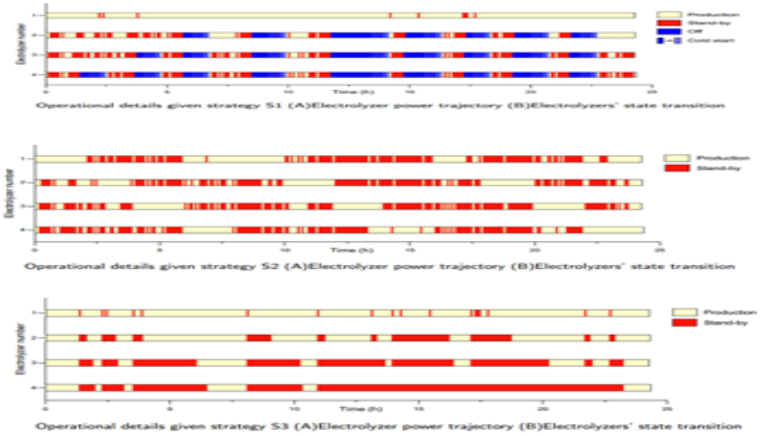

Figure 24 Performance of a multi-electrolyser system achieved under various operation strategies.

[C] X. Jin, S. You, et al., “Exploring Commercial Water Electrolyser Systems: A Data- based Analysis of Product Characteristics”, Clean Energy, 2023 (under review)

The analysis is based on publicly accessible data gathered from 28 WE manufacturers worldwide with a total of 186 products, focusing on technology types and various technical characteristics of each WE system, including capacity, conversion rate, footprint, hydrogen output pressure, hydrogen purity and efficiency. The analysis reveals that the current WE system solutions in the market exhibit diverse and varied characteristics. Such information can also be used for further design of the 1GW PtX system.

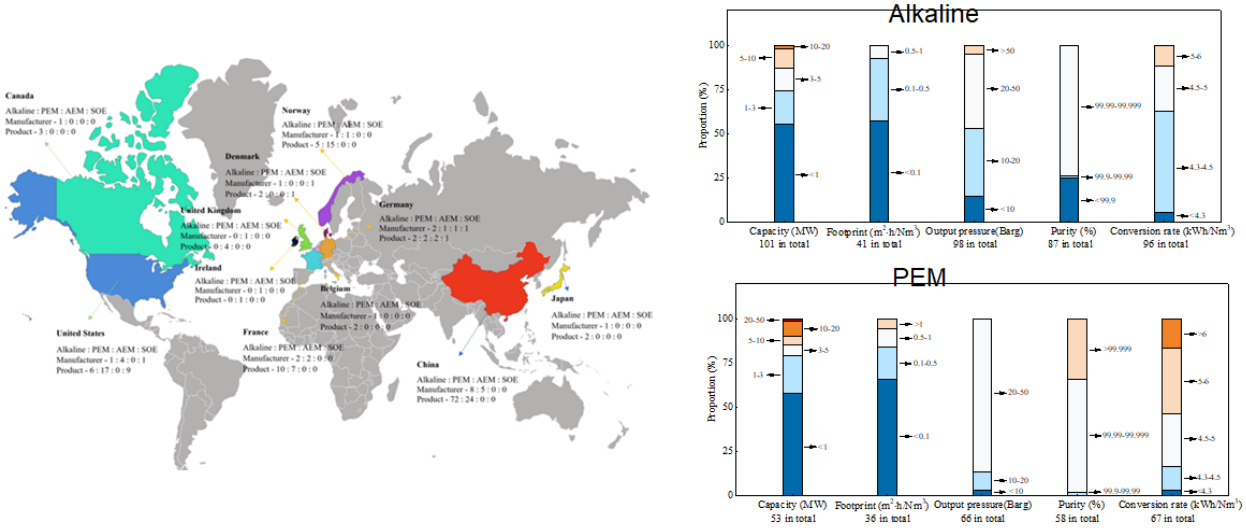

Figure 25 An overview of technical characteristics of global electrolyser products.

[D] Sergio Chen, “Techno-economic analysis of 1GW electrolyser portfolio for Energy Island Bornholm”, Master thesis project report, June 2023.

The thesis project carried out a techno-economic analysis for various 1GW electrolyser portfolios for Bornholm. Each portfolio consists of a number of identical electrolyser modules that use the same technology and have the same capacity. The analysis takes into account both the economic scaling effects and some operational aspects of the electrolyser portfolios (such as efficiency variation, various control strategies). The results offer a comprehensive overview of the techno-economic performance of different setups.

Table 4.3: Results for PEMEL simulations

		Scenario 2 1x1000	Scenario 4 5x
Technology		PEMEL	PEM
Control		Seq & Load	Sequer
Energy consumed		3,435,965	3,481,(
Energy curtailed/to grid	MWh	52,358	6,:
Energy required from grid	MWh	12,036	12,(
Energy balance with grid	MWh	40,321	- 5,(
Total H2 production	kg	64,561,821	62,859,(
Production rate	kg/h	7,390.37	7,195
Consumption rate	kWh/kg	53.22	55
Average usage 1 year	h/y	6,389.70	4,108
Average usage 20 years	h	127,794	82,
CAPEX	€	398,400,000	514,600,(
OPEX	€/y	11,952,000	15,438,(
OPEX stack	€	638,970,000	410,821,(
OPEX stack rounded	€	638,970,000	300,000,(
Total OPEX 1 year	€/y	43,900,500	35,979,(
Total OPEX 1 year rounded	€/y	43,900,500	30,438,(
OPEX 20 years rounded	€	878,010,000	608,760,(
CAPEX+OPEX	€	1,276,410,000	1,123,360,(

Scenario 4 Scenario 6 Scenario 6 Scenario 8 Scenario 8

Table 4.2: Results for AEL simulations

		Scenario 1 1x1000	Scenario 3 5x200	Scenario3 5x200	Scenario 5 10x100	Scenario 5 10x100	Scenario 7 50x20	Scenario 7 50x20
Technology		AEL	AEL	AEL	AEL	AEL	AEL	AEL
Control		Seq & Load	Sequential	Load	Sequential	Load	Sequential	Laod
Energy consumed		3,373,556	3,471,092	3,475,618	3,478,103	3,484,421	3,441,126	3,480,805
Energy curtailed/to grid	MWh	114,767	17,235	13,067	10,312	4,470	55,794	7,802
Energy required from grid	MWh	12,036	12,041	12,399	12,129	12,605	20,634	12,321
Energy balance with grid	MWh	102,731	5,194	668	- 1,817	- 8,135	35,160	- 4,519
Total H2 production	kg	67,068,142	66,459,329	66,548,401	66,150,248	66,275,868	65,084,274	65,923,697
Production rate	kg/h	7,677.27	7,607.58	7,617.78	7,572.20	7,586.58	7,450.18	7,546.27
Consumption rate	kWh/kg	50.30	52.23	52.23	52.58	52.57	52.87	52.80
Average usage 1 year	h/y	5,789.40	4,011.81	4,012.97	3,723.15	3,726.78	3,418.96	3,497.35
Average usage 20 years	h	115,788	80,236	80,259	74,463	74,536	68,379	69,947
CAPEX	€	357,700,000	481,800,000	481,800,000	547,500,000	547,500,000	730,000,000	730,000,000
OPEX	€/y	10,731,000	14,454,000	14,454,000	16,425,000	16,425,000	21,900,000	21,900,000
OPEX stack	€	347,364,000	240,708,800	240,778,200	223,388,800	223,607,000	205,137,400	209,840,860
OPEX stack rounded	€	270,000,000	108,000,000	108,000,000	108,000,000	108,000,000	86,400,000	86,400,000
Total OPEX 1 year	€/y	28,099,200	26,489,440	26,492,910	27,594,440	27,605,350	32,156,870	32,392,043
Total OPEX 1 year rounded	€/y	24,231,000	19,854,000	19,854,000	21,825,000	21,825,000	26,220,000	26,220,000
OPEX 20 years rounded	€	484,620,000	397,080,000	397,080,000	436,500,000	436,500,000	524,400,000	524,400,000
CAPEX+OPEX	€	842,320,000	878,880,000	878,880,000	984,000,000	984,000,000	1,254,400,000	1,254,400,000

Figure 26 Techno-economic analysis of a 1GW electrolyser portfolio with different configurations.

6. Conclusion and future work

Our research revealed key insights in different areas of the project. Below is a list of the key findings regarding different aspects of the feasibility study from an operational perspective,

Key findings – Electrolyser portfolio operation

- The purely wind-driven one GW electrolyser portfolio can have different configurations, such as 5x200MW vs. 20 X 50MW, resulting different performance.
- Difference in electricity consumption and hydrogen production as well as heat could be small, when the 1GW portfolio has a similar configuration.
- However, CAPEX and OPEX can be different for different configurations, which is investigated in another study.
- Number of start/stop of each module is different, which will influence lifetime and OPEX (briefly investigated in publication B, requires further investigation).
- Optimal operation can help to reduce the number of start/stop effectively (results are published in publication B), or powered by a more stable electricity source, e.g., a public grid.

Key findings – Power grid integration

- Excessive/residual wind power need to be curtailed or exported, which requires dedicated transmission lines, i.e., less than 2GW.
- Excessive /residual wind power profile is less fluctuating than the original 3GW wind power profile.
- Electrolysers can offer flexibility to the grid through dedicated control and operation strategies, if relevant.

Key findings – Heat recovery

- Though the amount of energy contained in waste heat is much larger than the demand of DH, the low temp. hinders direct use of the waste heat for DH. Further investigation on heat recovery methods and DH integration are necessary.

Key findings – Power to Ammonia

- A flexible operation of the synthesis plant (e.g., larger operation range and ramp rate) will help to produce more ammonia, when the hydrogen profile is non-stable and fluctuating.
- Storage of N2 and H2 can help to increase the overall flexibility (and deliver a stable gas supply to the synthesis plant), particularly when there is insufficient supply of H2. (A sizing analysis is recommended in future study)
- The complexity of dependencies among system components in dynamic processes requires further investigation of unit-commitment and operation strategies, particularly towards optimal operation.

Regarding the future investigation, we recommend design and development of pilot experimental setups or in-field small-scale commercial demonstration activities to validate the results from this study. Further, we recommend more detailed investigation on some particular subjects, such as waste heat recovery and utilization, in order to improve the efficiency and cost-effectiveness of the wind/electrolyser business.